Journal of Power Sources 387 (2018) 43–48

Contents lists available at ScienceDirect

Journal of Power Sources

journal homepage: www.elsevier.com/locate/jpowsour

A high-performance supercapacitor electrode based on N-doped porous graphene

Shuge Dai[a,b,1], Zhen Liu[c,1], Bote Zhao[b], Jianhuang Zeng[c,*], Hao Hu[b], Qiaobao Zhang[b], Dongchang Chen[b], Chong Qu[b], Dai Dang[b], Meilin Liu[b,**]

[a] School of Physical Engineering, Zhengzhou University, Zhengzhou, Henan, 450052, PR China
[b] School of Materials Science and Engineering, Georgia Institute of Technology, 771 Ferst Drive, Atlanta, GA, 30332-0245, United States
[c] School of Chemistry and Chemical Engineering, South China University of Technology, Guangzhou Key Laboratory for Surface Chemistry of Energy Materials, Guangdong Key Lab for Fuel Cell Technology, Guangzhou, 510641, PR China

HIGHLIGHTS

- N-doped graphene with 3D porous architecture was successfully prepared.
- The electrode delivered high specific capacitance and excellent cycling stability.
- The symmetrical supercapacitor achieved a remarkable energy and power density.

GRAPHICAL ABSTRACT

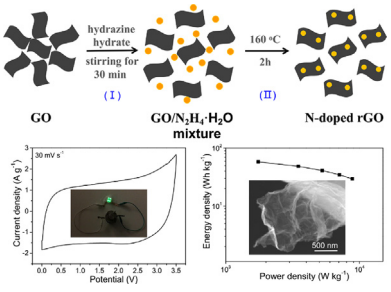

ARTICLE INFO

Keywords:
3D porous architecture
N-doped graphene
Supercapacitors

ABSTRACT

The development of high-performance supercapacitors (SCs) often faces some contradictory and competing requirements such as excellent rate capability, long cycling life, and high energy density. One effective strategy is to explore electrode materials of high capacitance, electrode architectures of fast charge and mass transfer, and electrolytes of wide voltage window. Here we report a facile and readily scalable strategy to produce high-performance N-doped graphene with a high specific capacitance (~390 F g^{-1}). A symmetric SC device with a wide voltage window of 3.5 V is also successfully fabricated based on the N-doped graphene electrode. More importantly, the as-assembled symmetric SC delivers a high energy density of 55 Wh kg^{-1} at a power density of 1800 W kg^{-1} while maintaining superior cycling life (retaining 96.6% of the initial capacitance after 20,000 cycles). Even at a power density as high as 8800 W kg^{-1}, it still retains an energy density of 29 Wh kg^{-1}, higher than those of previously reported graphene-based symmetric SCs.

1. Introduction

Graphene has attracted worldwide attention due to its unique electronic, thermal, mechanical, and catalytic properties [1–3]. It has been widely used as electrode materials for energy storage and conversion (e.g., supercapacitors, batteries, and fuel cells) [4–7]. The high specific surface area (~2630 m^2 g^{-1} for single sheet graphene) and its exceptional electronic properties make it appealing for supercapacitor

* Corresponding author.
** Corresponding author.
E-mail addresses: cejhzeng@scut.edu.cn (J. Zeng), meilin.liu@mse.gatech.edu (M. Liu).
[1] These authors contributed equally to this work.

https://doi.org/10.1016/j.jpowsour.2018.03.055
Received 8 February 2018; Received in revised form 19 March 2018; Accepted 21 March 2018

applications [8,9]. In principle, a supercapacitor based on graphene is capable of achieving a theoretical capacitance as high as 550 F g^{-1} (originated from electrochemical double layer) provided that the surface area is fully utilized [10,11]. However, the practical performance of graphene-based electrodes is far below the ideal one due to various reasons. For example, the strong Van der Waals interactions between adjacent graphene sheets greatly increase the tendency of re-stacking or aggregation of graphene sheets during fabrication processes, leading to reduced specific surface area, increased resistance to ions transport, and decreased number of active sites accessible to reactants [12–14].

Recently, numerous studies have shown that the electrochemical properties of graphene can be readily modified by doping [4]. Substitution of carbon atom by heteroatoms, particularly nitrogen, can effectively modulate its electronic characteristics, surface catalytic properties, and local chemical features, thus greatly enhancing the functionality and performances [15–17]. Moreover, doping graphene with nitrogen can not only improve the wettability and the accessibility of the active surface area to the electrolyte solution, but also enhance the electrical conductivity by enriching the free charge-carrier density [18]. To date, various routes have been developed to prepare N-doped graphene materials, including thermal treatment, solvothermal and superdoping methods [9,18–23]. However, all these approaches required high temperatures and were time-consuming. The fabricated supercapacitors (SCs), based on N-doped graphene electrodes, exhibit relatively low energy density, which hinders their large-scale practical applications [19–24]. Therefore, it is still a challenge to develop a simple, low-cost, and green method to produce high-quality N-doped graphene materials for SCs with high energy density, high power density, and long cycle life [25,26].

In this work, we focused on the development of high-performance symmetrical SC devices based on N-doped graphene electrodes. The electrochemical potential window of the devices is critical to achieving high energy density and power density for SCs. While the ionic liquid has a great advantage in obtaining wider operation potential windows, it also has high electrochemical stability. Here we report our findings in design and fabrication of a symmetrical SC device with a maximum operating voltage of 3.5 V using $BMIMBF_4$ as the electrolyte. The device demonstrated high energy density (55 Wh kg^{-1}) and excellent cycling stability (96.6% capacitance retention after 20,000 cycles), attributed primarily to the unique N-doped graphene electrode material (390 F g^{-1} at 1 A g^{-1}). The N-rGO material reduces the tendency for restacking of graphene sheets and creates 3-D porous structures composed of graphene sheets with interconnected open pores, thus providing an effective pathway for charge transport and high density of active sites for efficient ion adsorption/desorption. Furthermore, one such a SC device was used to power 4 commercial LEDs, demonstrating its potential application in energy storage systems.

2. Experimental section

2.1. Preparation of N-modified rGO and rGO samples

Graphene oxide (GO) was prepared from pristine graphite flakes using an improved Hummers' method [19]. The GO (100 mg) was dispersed in deionized water (37.5 mL) with continuous ultrasonicating for 2 h, which was then transferred into a 50 mL Teflon-lined stainless autoclave, followed by adding 2.5 g of hydrazine hydrate ($N_2H_4{\cdot}H_2O$) with continuous stirring for 30 min. Finally, the autoclave was sealed and maintained at 160 °C for 3 h. After cooling to room temperature naturally, the sample was rinsed with deionized water to make the pH = 7 and allowed to dry by freeze-drying. For comparison, the rGO sample was also prepared using the same procedure without the addition of hydrazine monohydrate.

2.2. Characterization

The phase structures of the samples were examined using X-ray diffraction (XRD) analysis (PAN'Alytical X'Pert Alpha 1, using Cu K-α1 X-rays). The microstructure and morphology of the products were observed using a scanning electron microscope (LEO 1530 field emission SEM) and a high resolution transmission electron microscope (JEOL JEM-2010HR, Japan). The electronic states of surface elements were characterized using X-ray photoelectron spectroscopy (Thermo K-Alpha XPS, Thermo Fisher Scientific). The nitrogen adsorption–desorption isotherm measurement of the samples was performed using a Micromeritics ASAP 2020 analyzer. The specific surface area was obtained by the Brunauer-Emmett-Teller (BET) method. Raman spectra were obtained using a Renishaw RM 1000 spectromicroscopy system (~2 μm spot size) equipped with a 20 × objective optical microscope.

2.3. Electrochemical measurement

Cyclic voltammetry (CV) and galvanostatic charge-discharge (GCD) tests were carried out using on a cell with a three-electrode configuration. The working electrode was composed of the active electrode material and a binder (PTFE) at a weight ratio of 9:1 (ethanol was used to form a uniform film). The typical areal mass loading of the active electrode material was approximately 2 mg cm^{-2}. The film electrode was then pressed between two nickel foams, and dried at 80 °C in vacuum for 12 h. A platinum mesh and a Ag/AgCl electrode (prefilled with 4 M KCl aqueous solution saturated with AgCl) were used as the counter and the reference electrodes, respectively. The electrochemical measurements of the supercapacitor were carried out to evaluate the N-doped graphene films for practical application in symmetric coin cells using two-electrode system in $BMIMBF_4$ electrolyte. Cyclic voltammograms were recorded on a Solartron electrochemical workstation (Solartron SI 1287 electrochemical interface). The galvanostatic charge/discharge measurements were performed using an Arbin testing system (BT-2143) at room temperature.

3. Results and discussion

The fabrication process for N-doped rGO (N-rGO) is schematically illustrated in Fig. 1. The structural features of the as-prepared N-rGO were characterized using XRD, Raman spectroscopy, XPS, and physical adsorption. As shown in Fig. 2a, all XRD patterns show two broad diffraction peaks at 26.3° and 43.3°, corresponding to (002) and (100) reflection, respectively. These results indicates that the pristine GO was successfully exfoliated into disordered and loosely packed graphene [27,28]. In the Raman spectra shown in Fig. 2b, the characteristic D-band (1326 cm^{-1}) and G-band (1585 cm^{-1}) were observed for the rGO and N-rGO. The intensity ratio of D-band to G-band (I_D/I_G) is an indication of the disorder degree of the graphene [4]. The value of I_D/I_G is 1.02 and 1.12 for rGO and N-rGO, respectively, suggesting that more defects were created by the nitrogen doping.

XPS was used to further examine the chemical composition of the prepared N-rGO sample. As shown in Fig. 2c, the XPS spectra for N-rGO exhibits a pronounced N1s peak located at 400.0 eV, indicating that nitrogen was successfully doped into the materials. The high-resolution

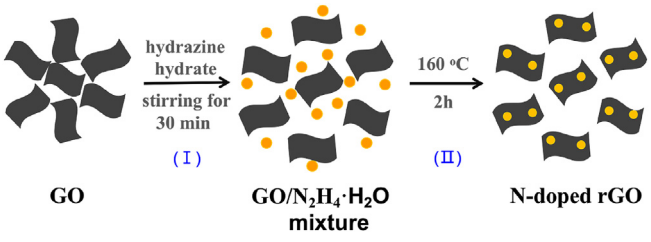

Fig. 1. Schematic diagram of preparing N-doped graphene material.

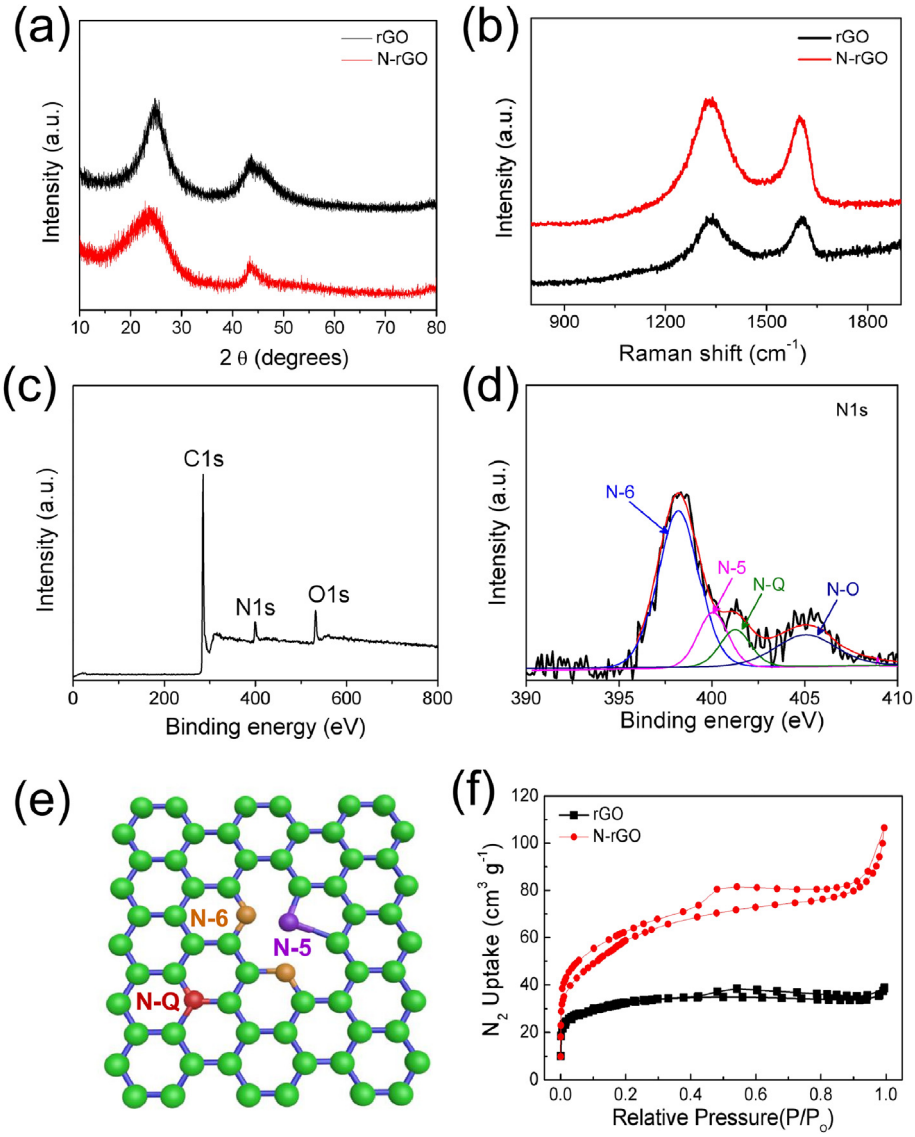

Fig. 2. (a) XRD patterns of rGO and N-rGO samples. (b) Raman spectra of rGO and N-rGO samples. (c) XPS spectra of N-rGO sample, and (d) N1s XPS spectra of N-rGO. (e) Possible locations for N incorporation into a fewlayer carbon network. (f) The nitrogen adsorption-desorption isotherms of rGO and N-rGO samples.

N1s spectrum (Fig. 2d) can be deconvoluted into four peaks centered at 398.3, 400.0, 401.2, and 404.9 eV, corresponding to the N-6 (pyridinic N), N-5 (pyrrolic N), N-Q (graphitic N), and N-O (oxidized N), respectively [22,29]. The significance of introducing N is that N-6 could lead to great pseudocapacitance effect and improve the conductivity, resulting in enhanced capacitive performance [4]. As shown in the schematic in Fig. 2e, N-6 indicates the doping where a nitrogen atom substitutes for a carbon atom in a hexagon, whereas N-5 represents the nitrogen atoms in a five-membered ring and thus contributing two electrons to the π-system [30,31]. N-Q is formed by substituting a carbon atom in a complete 2D honeycomb lattice. Moreover, N-6 and N-Q bond with two and three sp^2 C atoms, respectively, can contribute one pair of electrons to the conductive π-system [18]. Both of them can introduce one more electron to the π-system, which can be expected to greatly enhance the conductivity of rGO sheets [32,33]. More importantly, the high-level of the distributed N atoms can provide the N-rGO electrodes with both high density active sites and good wettability [18]. Besides, the N-Q groups can promote its interaction with the anions in the electrolyte and the formation of the electrical double layer, which can enhance the capacitance of SCs [32,34]. Therefore, this N-doped graphene material is expected to be a good candidate for high-performance SC electrodes. Nitrogen adsorption-desorption isotherms were used to provide more information on the porous structure of the functionalized graphene [5]. As shown in Fig. 2f, the N-rGO sample shows a large specific surface area of 203 $m^2 g^{-1}$, which is much higher than that of the rGO sample (111 $m^2 g^{-1}$). Moreover, the pore size distribution (Fig. S1) of N-rGO (5–9 nm) is wider than that of rGO (7–9 nm), and the higher pore volume of N-rGO relative to rGO is attributed to nitrogen doping, which reduces the agglomeration or restacking of graphene sheets and creates 3-D porous structures consisting of graphene sheets with interconnected open pores. The wide distribution of pore sizes is beneficial for energy storage where mesopores supply fast ion/electron transport with shorter diffusion/transport path.

The morphology and structure of the as-prepared N-rGO and rGO samples were also examined by SEM and TEM. It can be seen that N-rGO sample displays an interconnected porous network structure with wrinkles and curly edges (Fig. 3a and b). The interpenetrated network structure built from the N-rGO sheets was also observed in the TEM image (Fig. 3c), and the dark strips correspond to the folded edges or wrinkles of the nanosheets. In contrast, the rGO sample shows disordered and overlapping morphology (Fig. S2a); meanwhile, ultra-thin and flat graphene sheets are clearly visible in Fig. S2b. In addition, the

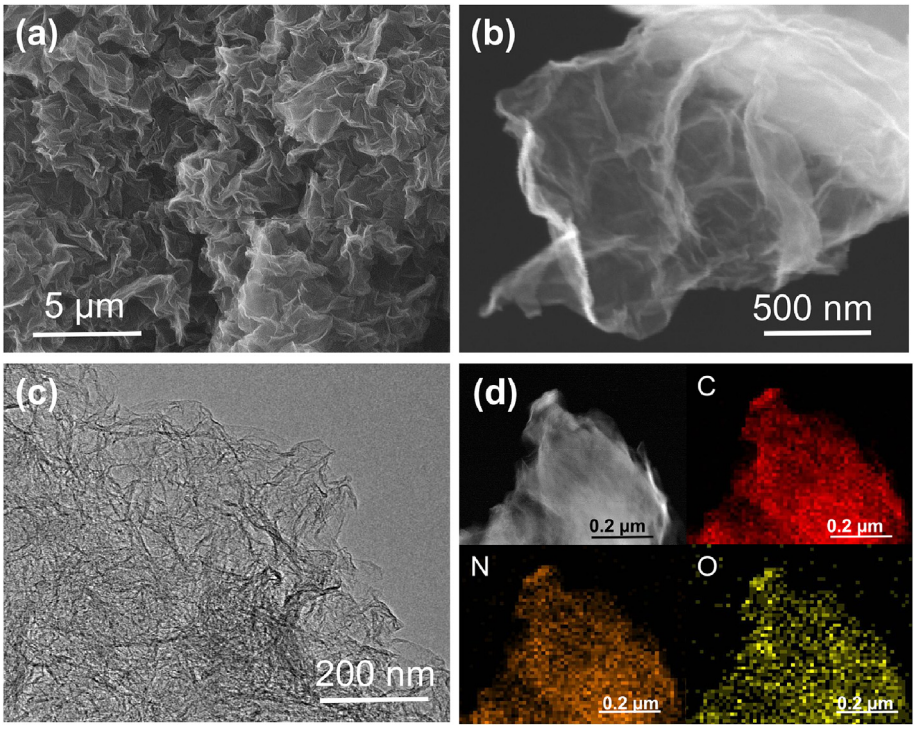

Fig. 3. (a,b) SEM images of N-rGO sample. (c) Low-magnification TEM image of N-rGO sample. (d) TEM-EDX mapping images of N-rGO sample.

corresponding TEM elemental mapping (Fig. 3d) performed on N-rGO shows that elemental C, N, and O are uniformly distributed, indicating that the nitrogen element has been doped into graphene sheets with high dispersion. Moreover, there is still small amount of oxygen in the N-rGO, which may originated either from the oxygen combined with nitrogen or from that doped into the carbon lattice which cannot be reduced completely by the hydrothermal treatment [22].

The electrochemical performances of the N-rGO as an electrode material for SCs were first investigated using cycle voltammetry (CV) and galvanostatic charge-discharge (GCD) in a test cell with three electrode configuration in 2.0 M KOH electrolyte. Fig. 4a displays the CV curves of rGO and N-rGO electrodes at a scan rate of 5 mV s^{-1}. It is obvious that N-doped graphene electrode exhibits much improved electrochemical performance compared to rGO. Fig. 4b shows the CV curves of N-rGO electrode at different scan rates in the potential range from 0 to −1 V; all curves exhibit approximately rectangular shapes, revealing the behavior of an electrical double-layer capacitor (EDLC). The corresponding CV curves of the rGO electrode were also collected and shown in Fig. S3a. Fig. 4c shows the representative GCD curves of the N-rGO electrode measured at different current densities. The curves display good symmetry and nearly linear discharge slopes, revealing the feature of EDLC as well. Moreover, no obvious voltage drop was observed, indicating relatively small internal resistance of the electrode. The calculated specific capacitance as a function of the discharge current density was plotted in Fig. 4d. It can be found that the specific capacitance of N-rGO electrode reaches 390 F g^{-1} at a current density of 1 A g^{-1}, which is 70% higher than that of the rGO electrode (207 F g^{-1}). Even at a high current density of 20 A g^{-1}, ~61% of the capacitance was still retained. To the best of our knowledge, the observed electrochemical performances are far superior to those reported for any N-doped carbon materials, including nitrogen/sulfur co-doped and hierarchical porous graphene hydrogels (251 F g^{-1}, 0.5 A g^{-1}) [35], N-doped graphene (312 F g^{-1}, 0.1 A g^{-1}) [4], p-phenylenediamine functionalized rGO (231 F g^{-1}, 0.5 A g^{-1}) [36], butane-1,4-diamine/rGO (208 F g^{-1}, 1 A g^{-1}) [5]. The excellent electrochemical performance of the N-rGO electrode may be attributed to the following reasons: (1) N-rGO electrode exhibits a large specific area that allows efficient ion adsorption/desorption; (2) Nitrogen incorporation can provide the N-rGO electrodes with high density active sites that promotes the capacitance performance. (3) The N-rGO material reduces the agglomeration level of graphene and creates few layer graphene sheets with interconnected open pores, which provides an effective pathway for charge transport. Moreover, the N-rGO electrode shows a lower interfacial resistance and faster ion diffusion near the electrode/electrolyte interface (Fig. S4).

To better illustrate the practical performance of N-rGO material, we constructed a symmetrical supercapacitor using two pieces of N-rGO with the same size and weight, tested in 1 M $BMIMBF_4$ electrolyte. Fig. 5a shows the CV curves of the N-rGO SC device at different scan rates within a potential window from 0 to 3.5 V. All CV curves retain nearly rectangular shapes with slight variations even at a scan rate as high as 200 mV s^{-1}, revealing excellent capacitive behavior of the N-rGO electrode. The representative GCD curves of the device measured at different current densities are shown in Fig. 5b. The discharge curves and the corresponding charge curves are nearly symmetrical; the nearly symmetrical triangular shape further implies excellent capacitive behavior of the SCs based on the N-rGO materials. The energy density and power density are two important parameters for evaluating the electrochemical behavior of the SCs [37,38]. As shown in the Ragone plot (Fig. 5c), the supercapacitor can deliver a high energy density of 55 W h kg^{-1} at a power density of 1.8 kW kg^{-1}. Even at a high power density of 8.8 kW kg^{-1}, it still retained an energy density of 29 W h kg^{-1}. The obtained energy densities are much higher than those of other previously reported symmetrical SCs based on similar electrode materials or electrolyte, including Tris/rGO (51 W h kg^{-1} at a power density of 552 W kg^{-1}) [5], hierarchically porous carbon (32 W h kg^{-1} at a power density of 620 W kg^{-1}) [39], carbon-graphene/MOF (30 W h kg^{-1} at a power density of 137 W kg^{-1}) [40], and N-doped graphene (27.4 W h kg^{-1} at a power density of 400 W kg^{-1}) [41].

The long-term cycling performance of the SC device was evaluated in a voltage window of 3.5 V at a current density of 10 A g^{-1} (Fig. 5d); it still retained ~96.6% of the initial capacitance after 20,000 cycles, revealing its excellent cycling stability. Furthermore, one SC device can power 4 commercial light-emitting diodes (LEDs) after being charged to

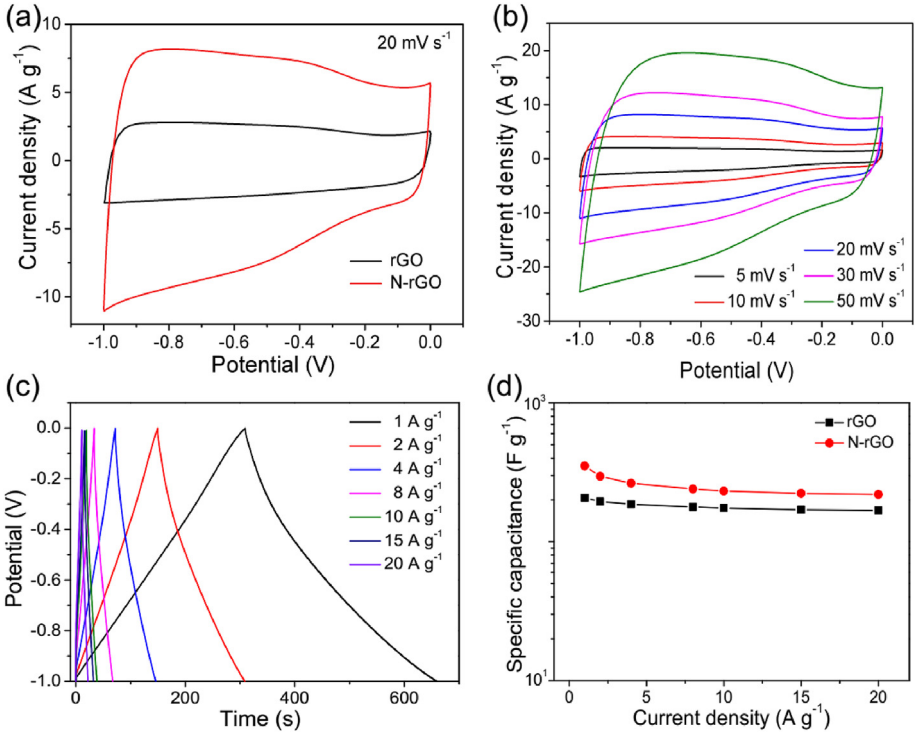

Fig. 4. (a) CV curves of rGO and N-rGO electrodes at scan rate of 20 mV s^{-1} (b) CV curves of N-rGO electrode at different scan rates. (c) GCD curves of N-rGO electrode at different charging-discharging current densities. (d) The specific capacitance of as-synthesized rGO and N-rGO samples.

3.5 V (Fig. 5d, Inset), demonstrating its viability and potential in practical applications (for detailed information, see corresponding video in supporting information).

Supplementary video related to this article can be found at http://dx.doi.org/10.1016/j.jpowsour.2018.03.055.

4. Conclusion

In summary, we have developed a simple and scalable process for synthesis of N-doped graphene with outstanding performance. The results suggest that the nitrogen atoms doped into the structure have effectively reduced the agglomeration of graphene sheets and created

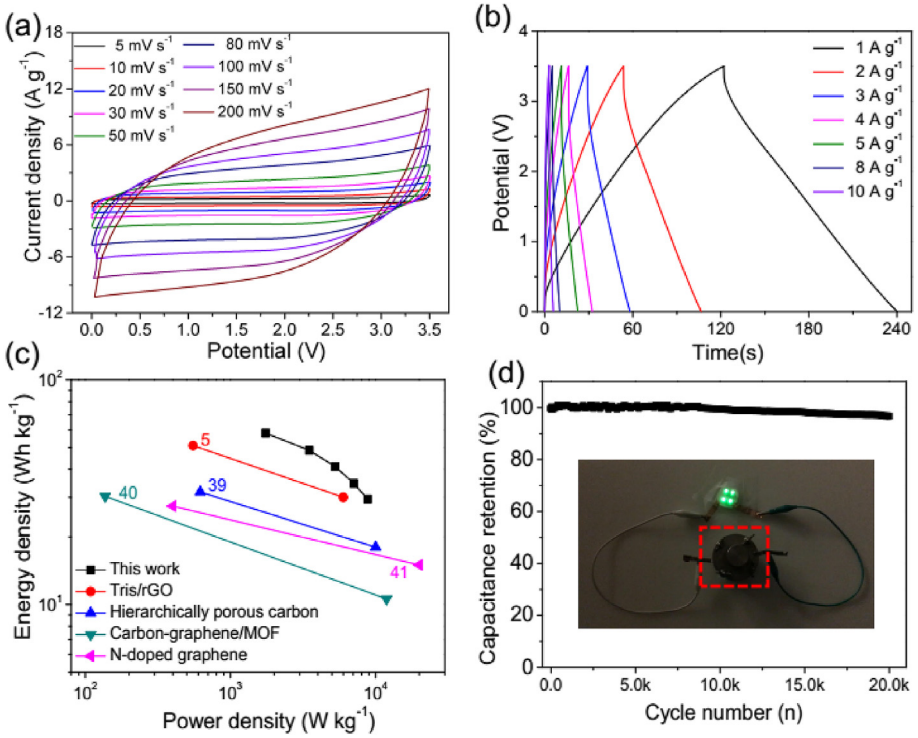

Fig. 5. (a) CV curves of N-rGO SC device at different scan rates. (b) GCD curves of N-rGO SC device at different charging-discharging current densities. (c) Ragone plots of the N-rGO SC. (d) Cycling performance of the SC. Inset shows the optical photograph of 4 LEDs lighted by one SC.

porous electrode structures composed of graphene sheets with interconnected open pores, greatly increasing the specific surface area of electrode materials and accelerating the ion transport. Moreover, a symmetrical SC device, constructed from N-rGO electrodes and $BMIMBF_4$ electrolyte, displayed a wide potential window (~3.5 V), high energy density (55 Wh kg^{-1}), and excellent cycling stability, demonstrating the viability and potential for energy storage applications. We believe that this unique N-rGO electrode is applicable to other energy storage and conversion systems.

Acknowledgements

This work was supported by the US National Science Foundation under award number DMR-1410320 and DMR-1742828, the Guangdong Innovative and Entrepreneurial Research Team Program (No. 2014ZT05N200), and the National Natural Science Foundation of China (51572090).

Appendix A. Supplementary data

Supplementary data related to this article can be found at http://dx.doi.org/10.1016/j.jpowsour.2018.03.055.

References

[1] C. Lee, X. Wei, J.W. Kysar, J. Hone, Science 321 (2008) 385–388.
[2] A. Fasolino, J.H. Los, M.I. Katsnelson, Nat. Mater. 6 (2007) 858–861.
[3] A.A. Balandin, S. Ghosh, W.Z. Bao, I. Calizo, D. Teweldebrhan, F. Miao, C.N. Lau, Nano Lett. 8 (2008) 902–907.
[4] K.L. Wang, M. Xu, Y. Gu, Z.G. Gua, J. Liu, Q.H. Fan, Nano Energy 31 (2017) 486–494.
[5] B. Song, J.X. Zhao, M.J. Wang, J. Mullaveya, Y.T. Zhu, Z.S. Geng, D.C. Chen, Y. Ding, K. Moon, M.L. Liu, C.P. Wong, Nano Energy 31 (2017) 183–193.
[6] D. Dang, H.B. Zou, Z. Xiong, S.Y. Hou, T. Shu, H.X. Nan, X.Y. Zeng, J.H. Zeng, S.J. Liao, ACS Catal. 5 (2015) 4318–4324.
[7] Z. Zhang, L.L. Kong, S. Liu, G.R. Li, X.P. Gao, Adv. Energy Mater. 7 (2017) 1602543.
[8] Y.B. Zhang, Y.W. Tan, H.L. Stormer, P. Kim, Nature 438 (2005) 201–204.
[9] L.S. Hua, X. Peng, Y. Li, L. Wang, K.F. Hu, L.Y.S. Lee, K.Y. Wong, P.K. Chub, Nano Energy 34 (2017) 515–523.
[10] M.F. El-Kady, V. Strong, S. Dubin, R.B. Kaner, Science 335 (2012) 1326–1330.
[11] Y.L. Shao, M.F. El-Kady, L.J. Wang, Q.H. Zhang, Y.G. Li, H.Z. Wang, M.F. Mousaviae, R.B. Kaner, Chem. Soc. Rev. 44 (2015) 3639–3665.
[12] H. Li, Y. Tao, X.Y. Zheng, J.Y. Luo, F.Y. Kang, H.M. Cheng, Q.H. Yang, Energy Environ. Sci. 9 (2016) 3135–3142.
[13] X.Z. Zhou, Z.Y. Bai, M.J. Wu, J.L. Qiao, Z.W. Chen, J. Mater. Chem. A 3 (2015) 3343–3350.
[14] C. Li, G. Shi, Adv. Mater. 26 (2014) 3992–4012.
[15] Y.B. Zhang, T.T. Tang, C. Girit, Z. Hao, M.C. Martin, A. Zettl, M.F. Crommie, Y.R. Shen, F. Wang, Nature 459 (2009) 820–823.
[16] X.L. Li, H.L. Wang, J.T. Robinson, H. Sanchez, G. Diankov, H.J. Dai, J. Am. Chem. Soc. 131 (2009) 15939–15944.
[17] Z.H. Xiang, D.P. Cao, L. Huang, J.L. Shui, M. Wang, L.M. Dai, Adv. Mater. 26 (2014) 3315–3320.
[18] W.L. Zhang, C. Xu, C.Q. Ma, G.X. Li, Y.Z. Wang, K.Y. Zhang, F. Li, C. Liu, H.M. Cheng, Y.W. Du, N.J. Tang, W.C. Ren, Adv. Mater. 29 (2017) 1701677.
[19] B. You, L. Wang, L. Yao, J. Yang, Chem. Commun. 49 (2013) 5016–5018.
[20] Y. Lu, F. Zhang, T. Zhang, K. Leng, L. Zhang, X. Yang, Y. Ma, Y. Huang, M. Zhang, Y. Chen, Carbon 63 (2013) 508–516.
[21] Y. Liu, Y.T. Shen, L.T. Sun, J.C. Li, C. Liu, W.C. Ren, F. Li, L.B. Gao, J. Chen, F. Liu, Y.Y. Sun, N.J. Tang, H.M. Cheng, Y.W. Du, Nat. Commun. 7 (2016) 10921.
[22] Y. Qing, J. Yuan, Juan Li, D.C. Chen, Y. Kong, F.Q. Chu, Y.X. Tao, M.L. Liu, Adv. Mater. 27 (2015) 5171–5175.
[23] M. Kota, X. Yu, S.H. Yeon, H.W. Cheong, H.S. Park, J. Power Sources 303 (2016) 372–378.
[24] W. Xia, C. Qu, Z.B. Liang, B.T. Zhao, S.G. Shu, B. Qiu, Y. Jiao, Q.B. Zhang, X.Y. Huang, W.H. Guo, D. Dang, R.Q. Zou, D.G. Xia, Q. Xu, M.L. Liu, Nano Lett. 17 (2017) 2788–2795.
[25] Z. Li, J. Liu, K. Jiang, T. Thundat, Nano Energy 25 (2016) 161–169.
[26] B. Mendoza-Sánchez, Y. Gogotsi, Adv. Mater. 28 (2016) 6104–6035.
[27] L. Stobinski, B. Lesiak, A. Malolepszy, M. Mazurkiewicz, B. Mierzwa, J. Zemek, P. Jiricek, I. Bieloshapka, J. Electron. Spectrosc. Relat. Phenom. 195 (2014) 145–154.
[28] Y. Han, Y. Wu, M. Shen, X. Huang, J. Zhu, X. Zhang, J. Mater. Sci. 48 (2013) 4214–4222.
[29] Y.F. Zhao, S.F. Huang, M.R. Xia, S. Rehman, S.C. Mu, Z.K. Kou, Z. Zhang, Z.Y. Chen, F.M. Gao, Y.L. Hou, Nano Energy 28 (2016) 346–355.
[30] Z.Q. Tan, K. Ni, G.X. Chen, W.C. Zeng, Z.C. Tao, M. Ikram, Q.B. Zhang, H.J. Wang, L.T. Sun, X.J. Zhu, X.J. Wu, H.X. Ji, R.S. Ruoff, Y.W. Zhu, Adv. Mater. 29 (2017) 1603414.
[31] W. Ren, D.J. Li, H. Liu, R. Mi, Y. Zhang, L. Dong, L. Dong, Electrochim. Acta 105 (2013) 75–82.
[32] Y.F. Deng, Y. Xie, K.X. Zou, X.L. Ji, J. Mater. Chem. A 4 (2016) 1144–1173.
[33] Y. Liu, Y.T. Shen, L.T. Sun, J.C. Li, C. Liu, W.C. Ren, F. Li, L.B. Gao, J. Chen, F. Liu, Y.Y. Sun, N.J. Tang, H.M. Cheng, Y.W. Du, Nat. Commun. 7 (2016) 10921.
[34] O. Ornelas, J.M. Sieben, R. Ruiz-Rosas, E. Morallon, D. Cazorla-Amoros, J. Geng, N. Soin, E. Siores, B.F. Johnson, Chem. Commun. 50 (2014) 11343–11346.
[35] J.H. Li, G.P. Zhang, C.P. Fu, L.B. Deng, R. Sun, C.P. Wong, J. Power Sources 345 (2017) 146–155.
[36] X.N. Lu, L.Y. Li, B. Song, K. Moon, N.N. Hu, G.L. Liao, T.L. Shi, C.P. Wong, Nano Energy 17 (2015) 160–170.
[37] S.G. Dai, B. Zhao, C. Qu, D.C. Chen, D. Dang, B. Song, B. deGlee, J.W. Fu, C.C. Hu, C.P. Wong, M.L. Liu, Nano Energy 33 (2017) 522–531.
[38] S.G. Dai, W.N. Xu, Y. Xi, M.J. Ming, X. Gu, D.L. Guo, C.G. Hu, Nano Energy 19 (2016) 363–372.
[39] P. Cheng, S.Y. Gao, P.Y. Zang, X.F. Yang, Y.L. Bai, H. Xu, Z.H. Liu, Z.B. Lei, Carbon 93 (2015) 315–324.
[40] L. Wang, T. Wei, L.Z. Sheng, L.L. Jiang, X.L. Wu, Q.H. Zhou, B. Yuan, J.M. Yue, Z. Liu, Z.J. Fan, Nano Energy 30 (2016) 84–92.
[41] P. Hao, Z.H. Zhao, Y.H. Leng, J. Tian, Y.H. Sang, R. Boughton, C.P. Wong, H. Liu, B. Yang, Nano Energy 15 (2015) 9–23.